

pubs.acs.org/journal/apchd5 Article

Strong-Field Control of Plasmonic Properties in Core—Shell Nanoparticles

Jeffrey A. Powell,* Jianxiong Li,* Adam Summers, Seyyed Javad Robatjazi, Michael Davino, Philipp Rupp, Erfan Saydanzad, Christopher M. Sorensen, Daniel Rolles, Matthias F. Kling, Carlos Trallero, Uwe Thumm, and Artem Rudenko



Cite This: ACS Photonics 2022, 9, 3515-3521



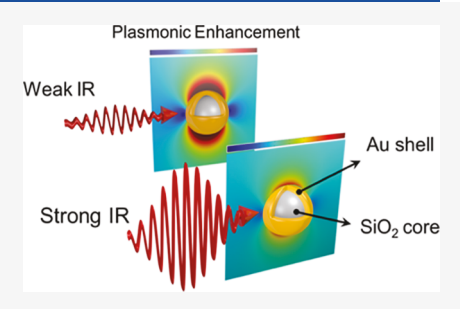
ACCESS

Metrics & More

Article Recommendations

Supporting Information

ABSTRACT: Utilization of the plasmonic response in nanosystems is a key component of nanophotonics that is typically altered by varying the incident optical frequency or the material configuration. However, in this work we demonstrate that employing intense, femtosecond laser fields unlock nonlinear light—matter interactions such that precise control of the optical response is achieved solely by adjusting the incident intensity. The plasmonic properties of ${\rm Au/SiO_2}$ nanoshells are manipulated by exploiting the nonlinear index of refraction of gold and experimentally observed by employing photoelectrons emitted during the interaction as a sensitive, sub-wavelength probe. A striking transition seen in the photoelectron energy spectrum between the weak and strong-field regime is verified by a modified Mie theory simulation that incorporates the nonlinear dielectric



nanoshell response. The exhibited intensity-dependent optical control of the plasmonic response in prototypical core—shell nanoparticles paves the way toward ultrafast switching and opto-electronic signal modulation with more complex nanostructures.

KEYWORDS: nanoplasmonics, femtosecond laser, nonlinear optics, photoelectron spectroscopy

■ INTRODUCTION

The ability to reversibly manipulate the electronic structure and optical response of nanometer-sized materials has recently attracted substantial attention. 1-3 A hallmark property of nanostructures is the capacity to design and fabricate systems to take advantage of the tunable, size-, shape-, frequency-, and material-dependent properties as a means of tailoring specific optical responses. This holds promise to both further our understanding of the transient electronic response in solid matter as well as enable new applications such as novel optoelectronics,³ plasmonically enhanced light harvesting,⁴ and photocatalysis.^{5,6} Among different configurations, composite nanostructures, such as core-shell nanoparticles, consisting of a dielectric core and a thin metallic shell, are of special interest for their exceptionally large plasmonic field enhancement and high tunability of absorption spectra, 7,8 generating novel applications in optical imaging and photothermal cancer therapy.^{9,10} Precise control of the optical response, typically achieved by manipulating the geometric structures,8 is key to utilizing their unique plasmonic properties.

Investigations into such optical properties in nanostructures have been conducted by studying their plasmonic response, in particular, their plasmonic near-field enhancement.^{7,11–14} For intense laser fields, the use of photoelectrons provides an excellent window into understanding of the dynamics of these interactions due to their sensitivity on the sub-wavelength spatial and ultrafast temporal scales, especially to the transient-induced plasmonic field distribution. Photoelectron spectros-

copy utilizes photoelectrons emitted during the interaction of a nanoparticle with an intense, femtosecond laser, allowing for the unraveling of the fundamental contributions to their acceleration, including enhanced near-fields, surface rescattering, and charge interactions. Experiments revealed the fundamental light-matter interaction processes during the optical response and associated electron dynamics in selected nanosystems (nanospheres, nanotips), consistent with theoretical modeling of the induced plasmonic field near the nanostructure surface in the linear response approximation. $^{17-23}$

Recent investigations of nanoscale thin films and metasurfaces have revealed significant nonlinear (Kerr) effects^{24,25} and demonstrated the possibility to use such effects to optically manipulate the plasmonic properties in various nanostructures.²⁶ Therefore, a compelling interest is raised to utilize nonlinear effects for the optical control of the plasmonic properties of the aforementioned composited nanostructures, especially those with thin layers such as core—shell nanoparticles. Here, we investigate a type of core—shell nanoparticle

Received: May 2, 2022 Published: October 28, 2022





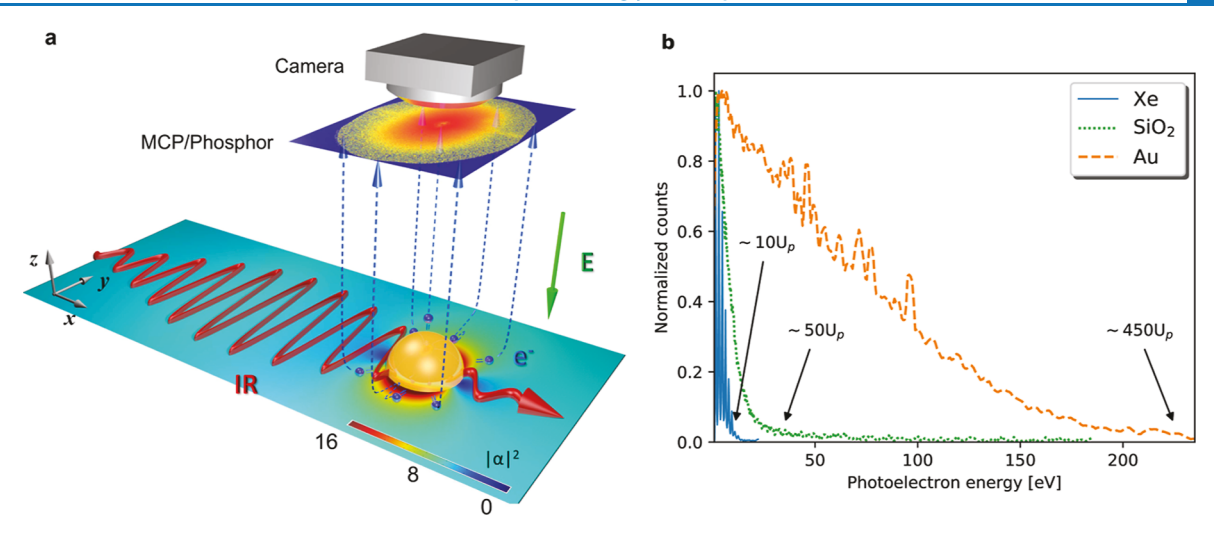


Figure 1. Experimental schematic and photoelectron energy spectra. (a) Schematic of an ultrafast laser interaction with a single, isolated nanoparticle in vacuum. The emitted photoelectrons are angle- and energy-resolved using high-energy VMI spectroscopy. (b) Comparison of the obtained photoelectron energy distribution for photoemission from gaseous Xe (blue solid line), 120 nm diameter SiO_2 nanospheres (green dotted line), and 120 nm diameter Au nanospheres (gold dashed line), at a peak laser intensity of 8 TW/cm² at 780 nm wavelength. Respective cutoff energies in units of the ponderomotive energy U_p are indicated by arrows. All spectra are obtained from photoelectron counts within a 30° cone centered along the polarization direction.

specifically tailored to have a significant nonlinear optical response which enables the intensity-dependent optical control of its plasmonic properties. This core-shell nanoparticle is composed of a nanometer-thin gold coating encasing a larger dielectric silica core. We demonstrate, experimentally and theoretically, that, as a function of the incident field intensity, a nonlinear response in the gold shell can be induced to control the plasmonic properties of the nanoparticle. At laser intensities below 0.1 TW/cm², the linear response dominates, resulting in a large plasmonic near-field. However, with increasing intensity, the onset of a nonlinear component of the complex index of refraction for gold decreases the skin depth and effectively reduces the magnitude of the near-field. This ability to manipulate the plasmonic properties of coreshell nanoparticles solely by tuning the external-field intensity substantiates a new method of precise control over the optical response in layered nanomaterials.

METHODS

Experimental Setup. The experiment was performed at the James R. Macdonald Laboratory at Kansas State University making use of a Ti:sapphire-based chirped pulse amplification system generating 25 fs pulses at 780 nm central wavelength. Photoelectron spectra were captured using a thick-lens, highenergy velocity map imaging (VMI) spectrometer²⁷ capable of gathering up to 350 eV electron energy. The custom nanoparticle source produces a continuous beam of nanoparticles into vacuum. Spherical nanoparticle samples were selected for their narrow size distribution and overall purity. The initial nanoparticle concentration was also carefully chosen to avoid the formation of clusters in the nanoparticle beam.

Laser Intensity Characterization. The peak laser intensity was determined by analyzing the above-threshold ionization photoelectron energy distribution of atomic Xe with the aforementioned VMI under similar experimental parameters. The ponderomotive shift of the Xe above-threshold ionization comb was measured as a function of the input laser pulse energy, in order to derive the ponderomotive energy $U_{\rm p}$

 $\propto I\lambda^2$ and thus, the peak laser intensity $I.^{28,29}$ For intensities below the ionization threshold of Xe, the ratio of the pulse energies was used to extrapolate the peak intensity. See Note S1 for more details.

Photoelectron Cutoff Determination. The nanoparticle photoelectron cutoff energy was extracted from the experimental VMI images in a method described in a previous work. The detected elastically back-scattered photoelectrons are obtained from the non-inverted VMI images, for which the upper energy boundaries of the full 3D momentum sphere and the 2D projection are essentially the same. A radial distribution of these projections along the polarization direction accurately determines the maximum photoelectron energy.

Mie Simulations. We simulated laser-induced plasmonic near-fields by solving the Mie equations^{30,31} for plane waves scattered by spherical objects. The linear terms of the dielectric response of Au and SiO₂ enter as the frequency-dependent complex-valued index of refraction obtained from experiments.^{32,33} Our inclusion of nonlinear effects is discussed in the next section. As the original Mie theory applies only to the solid spheres, we used a modified Mie theory to simulate the plasmonic near-fields of core—shell structures,^{34,35} as outlined in Note S3.

RESULTS AND DISCUSSION

Probing Plasmonic Field Enhancement. The photo-electron cutoff energy, defined as the highest observable electron energy, has been established as a gold standard for probing the induced plasmonic near-fields close to various nanostructure surfaces of different materials. 12,13,36,37 This cutoff scales linearly with the cycle-averaged quiver energy of a free electron in a laser field, referred to as the "ponderomotive energy" $U_p = e^2 E^2 / 4m\omega^2 \propto I\lambda^2$ (e and m are electron charge and mass and E, I, ω , and λ designate the incident field strength, peak intensity, frequency, and wavelength of the laser pulse, respectively). Though near-fields are generally inhomogeneous (decreasing with distance), the fastest photoelectrons elastically rescatter and gain most of their kinetic energies near

the nanoparticle surface, 17,28 well within the typical spatial range of the near-field enhancement. 7,28,38 Therefore, rescaling photoelectron cutoff energies with the incident field $U_{\rm p}$ reveals information about the plasmonic near-field enhancements, independent of the incident-field intensity.

We determine the cutoff energies for single, isolated nanoparticles photoionized by femtosecond laser pulses, employing a high-energy VMI spectrometer to measure the energy- and angle-resolved photoelectron spectra (see Methods for additional details). Figure 1a illustrates a simplified schematic of the interaction and subsequent electron propagation and detection. Figure 1b shows the comparison of typical photoelectron energy spectra and their respective cutoff energies for atomic Xe, SiO₂ nanospheres, and Au nanospheres, exemplifying the substantial increase in the kinetic energy of electrons emitted from nanoparticles.

To demonstrate the feasibility of observing the signature of the near-field in these nanosystems, we measured the sizedependent photoelectron cutoff energies for solid Au nanospheres. Figure 2a shows the cutoff energies for diameters

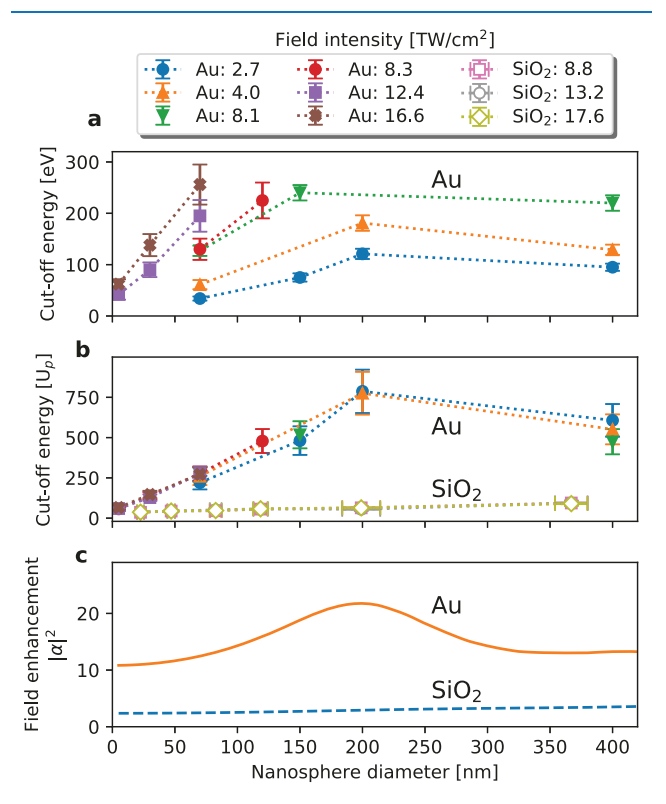


Figure 2. Probing field enhancements with photoelectron cutoff energies. (a) Size-dependent maximum cutoff energies from experimental VMI spectra for various laser intensities for Au nanospheres in units of eV and for an incident pulse wavelength of 780 nm. (b) Same cutoff energies as in (a) for Au and SiO₂ nanospheres rescaled to incident-field ponderomotive energy U_p . (c) Simulated near-field enhancement $|\alpha|^2$ for Au (orange solid line) and SiO₂ nanospheres (blue dashed line).

ranging from 5 to 400 nm at several intensities. The plasmonic near-field response was investigated by rescaling the cutoff energies to their respective incident-field ponderomotive energy $U_{\rm p}$ as shown in Figure 2b. For comparison, the cutoff energies for SiO₂ nanospheres at similar diameters and intensities are also plotted. The $U_{\rm p}$ -rescaled cutoff energies for both materials are shown to be independent of the laser

field intensity, within the size and intensity range of this work, as evidenced in Figure 2b by the overlap of the data points for each particular size. The cutoff energies for Au nanospheres indicate a prominent peak at diameter D=200 nm and more energetic photoelectrons than for SiO_2 nanoparticles, for which only a slight, monotonic increase with diameter occurs.

Further analysis in Figure 2c reveals that the U_p -rescaled cutoff energies resemble the maximum near-field intensity enhancement (which we refer to as "field enhancement" $|\alpha|^2$), in Figure 2b. For the results shown in Figure 2c, we calculated the induced near-field by numerically solving the Mie equations^{30,31} using indices of refraction within the linear optical response for Au and SiO₂ nanospheres.³² The field enhancement is defined by the maximum total field intensity with respect to the incident intensity and typically located close to the particle surface. ^{22,39} Though the exact dependence between the cutoff energy and field enhancement is determined by multiple effects (such as rescattering and Coulomb interactions)^{15,17}Figure 2b,c reveals that the cutoff energy does, nevertheless, accurately reflects the dominant signature of field enhancement profiles for Au and SiO₂ nanospheres (see Note S2). This agreement supports our use of the cutoff energy as an indicator for observing changes in the magnitude of the plasmonic field enhancement.

Controlling Plasmonic Properties in Core-Shell Structures. To investigate the strong-field control of the plasmonic properties in a layered nanostructure, we examined SiO₂-core-Au-shell structures. Core-shell nanoparticles were specifically chosen to elucidate any intensity-related changes to the field enhancement due to their unique configuration in comparison with solid Au nanospheres of a comparable size. The nanometer-thin Au shell surrounding a dielectric core results in a stronger localization of the plasmonic near-field when compared to solid Au nanospheres. We neglect any laserinduced propagation effects as the nanoparticle radius is much smaller than the incident pulse wavelength. Figure 3a shows our measured intensity-dependent photoelectron cutoff energies, rescaled with the incident-field ponderomotive energy U_p at 780 nm wavelength, for core-shell structures and solid Au nanospheres of approximately 150 nm diameter.

The U_p -rescaled cutoff energy for solid Au nanospheres remains approximately unchanged ($\sim 500U_p$) for different incident-field intensities, indicating that the field enhancement near solid Au nanospheres is nearly independent of the intensity (Figure 3a). In contrast, the cutoff energy for the core-shell structures varies drastically within the intensity range sampled. At low intensities, this energy is large when scaled by U_p (~2500 U_p , approximately 10 eV). However, it rapidly decreases and converges to the nearly identical value of the solid Au nanospheres beyond $\sim 2 \text{ TW/cm}^2$, as indicated by the black arrow in Figure 3a. This implies that the field enhancement of the core-shell structure does not remain constant with the increasing laser intensity, but rather begins (at low intensity) at a significantly larger value than the enhancement of solid Au nanospheres, before quickly decreasing to a similar value at higher intensities. The contrast of these two particles is particularly strong at very low intensities (~ 0.1 TW/cm²), where no photoemission is observed for solid Au nanospheres due to the extremely weak electromagnetic field. A measurable amount of photoelectrons with over $2000U_p$ cutoff energy are still observed from core-shell structures, further confirming that a large field enhancement is induced at low intensities.

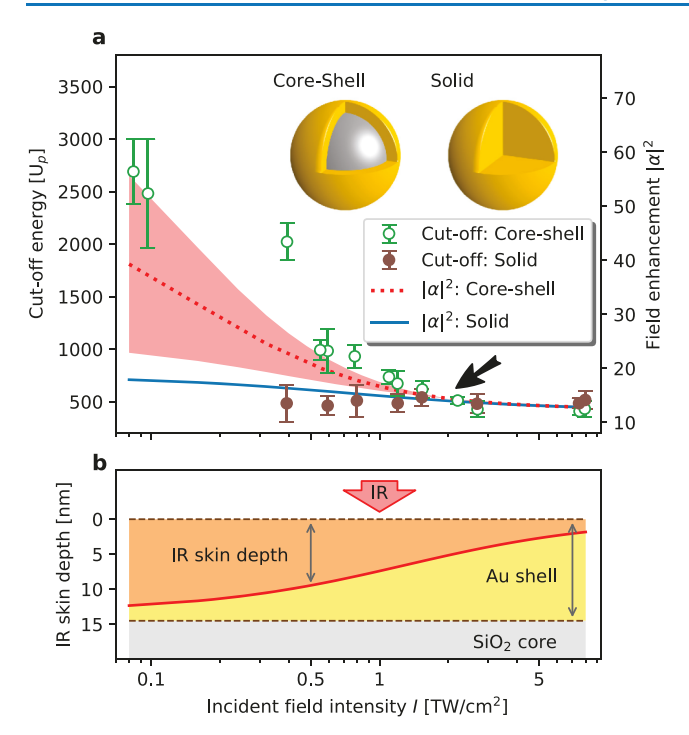


Figure 3. Probing and analyzing intensity-dependent field enhancement of core-shell structures and solid Au nanospheres. (a) Maximum photoelectron cutoff energies in the units of incidentfield ponderomotive energy U_p for SiO_2 -core-Au-shell structures (hollow markers) and solid Au nanospheres (solid markers), as a function of the incident-field intensity I. The core-shell structures have an outer diameter D_2 = 147 \pm 7 nm and an inner diameter D_1 = 118 ± 4 nm whereas the solid Au nanospheres have a diameter of 150 \pm 5 nm. The simulated field enhancement $|\alpha|^2$ (scale on the right) for core-shell structures (red dotted line) and solid Au nanospheres (blue solid line) are also plotted for comparison. The red shaded area is the calculated uncertainty range caused by the manufacturing dispersity of the inner and outer radii of the core-shell structures (see Note S4). The black arrow indicates the selected convergence of the core-shell and solid nanospheres in cutoff energies and in field enhancements. (b) Calculated IR skin depth (red line and darkened area) for a Au shell thickness of 14.5 nm, as a function of the incidentfield intensity I. All results are for an incident pulse wavelength of 780 nm.

Physical Mechanism of Strong-Field Control. The nonlinear optical response of the Au shell is the key to understanding the observed effects in core—shell nanoparticles. Note that only the linear optical response is included in Figure 2c. To include the nonlinear response, we apply a simple and widely used model to account for intensity-dependent changes in the index of refraction for Au⁴⁰

$$n = n_0 + n_2 I \tag{1}$$

where n_0 , an experimentally determined complex number,³² is the linear index of refraction employed for our simulation results in Figure 2. n_2 is related to the third-order susceptibility $\chi^{(3)}$ (or the Kerr effect)⁴¹

$$n_2 (\text{m}^2/\text{W}) = \frac{283}{n_0 \Re(n_0)} \chi^{(3)} (\text{m}^2/\text{V}^2)$$
 (2)

 $\Re(n_0)$ is the real part of n_0 and $\chi^{(3)} = (-9.1 + 0.35i) \times 10^{-19}$ m²/V², according to a measurement using 15 nm Au films, ⁴² close to the Au shell thickness in our work. At 780 nm wavelength, $n_2 = (0.026 + 3.65i) \times 10^{-12} (\text{W/cm}^2)^{-1}$ is pre-

dominantly imaginary. When I \rightarrow 0, the linear optical response dominates and $n \approx n_0$. As the intensity increases, the imaginary part $\mathfrak{F}(n) = \mathfrak{F}(n_0) + \mathfrak{F}(n_2) \times I$ increases, and the nonlinear effect starts to emerge.

We estimate the normal incident IR skin depth σ following ⁴³ as

$$\sigma = \frac{c}{2\omega \mathfrak{T}(n)} = \frac{c}{2\omega [\mathfrak{T}(n_0) + \mathfrak{T}(n_2) \times I]}$$
(3)

where c is the speed of light. Thus, the IR skin depth decreases with incident-field intensity in this particular situation. Figure 3b plots the intensity-dependent IR skin depth, in comparison with the Au shell thickness (~14.5 nm) of the core-shell structures. At low intensities (<0.1 TW/cm²), the skin depth is approximately 13 nm, comparable to the Au shell thickness, suggesting that a considerable amount of the IR field reaches the SiO₂ core. Because the optical response of a core-shell nanoparticle is extremely sensitive to the fields at both the inner and outer surfaces, their larger field enhancement results from the penetration of the external field into the Au-SiO₂ interface. This effect is incorporated by applying the boundary conditions at both interfaces when solving the Mie equations. However, as the intensity increases, σ rapidly drops and approaches 2 nm at 8 TW/cm², well below the Au-shell thickness, preventing the IR field from penetrating the Au shell, that is, shielding the SiO2 core. Therefore, the outer Au surface becomes the dominant factor for determining the optical response (and thus the field enhancement), causing the core-shell structures to appear to be indistinguishable from solid Au nanospheres of the same outer diameter.

Note that, while a recent study included the nonlinear response of SiO₂ nanoparticles, ¹⁸ we neglect such effects in the SiO₂ core of the core-shell structures because the field near the Au-SiO₂ interface is too heavily dampened (not exceeding 10¹⁰ W/cm²) to induce any significant nonlinear response in this study. In addition, we point out that the macroscopic theoretical model given by eq 1 is incomplete with regard to two aspects. (i) It lacks the detailed self-consistent description of the nanoparticle's electronic response to and ensuing modification of the external laser electric field. Such a comprehensive microscopic numerical modeling of the laser-matter interaction would require the self-consistent solution of Schrödinger's and Maxwell's equations and is clearly beyond the scope of the present investigation. $^{44-46}$ (ii) We assume the intensity-independent nonlinear response coefficient n_2 in eq 1 is perturbative and thus valid near the onset of nonlinear refraction. This assumption will fail for high intensities in the strongly nonlinear regime. Our model based on eq 1 is nevertheless able to capture the onset and characteristics of the observed nonlinear effect on photoelectron emission due to the first nonlinear corrective term, n_2I . In fact, as discussed below, the intensity-dependent transition from linear to nonlinear response is revealed in the experimental cutoff energies and agrees with the physically transparent modeling in eq 1.

Figure 3a also plots the Mie-simulated field enhancement $|\alpha|^2$ for core—shell structures and solid Au nanospheres, including the nonlinear optical response. The field enhancement of solid Au nanospheres only decreases slightly from 18 to 13 as the intensity increases. This indicates that the nonlinear response, while present in solid Au nanospheres, is insignificant and does not induce a measurable difference exceeding experimental uncertainty in this work, justifying our

calculation of the results in Figure 2 using a linear response approximation. The core-shell structures, on the other hand, start with a field enhancement up to 60 at low intensities, where linear response dominates. This large enhancement is responsible for the photoemission observed from core-shell structures at low intensities, which is absent in solid Au nanospheres, as well as the significantly larger cutoff energy. As the intensity increases, the nonlinear response results in a decreasing skin depth (Figure 3b), leading to significantly smaller field enhancements that eventually converge with our results for the solid Au nanospheres beyond ~2 TW/cm². The profiles of the simulated field enhancements, especially the convergence at ~2 TW/cm², are in excellent agreement with that of the measured cutoff energies for both nanoparticles. This success validates the use of the simple model in eq 1 and shows that the laser intensity has a significant impact on the plasmonic response of core-shell structures, in contrast to their solid Au counterparts.

A more in-depth understanding of the intensity-dependent plasmonic response and its broader implications can be achieved by extending our line of investigation to a larger spectral range. Figure 4d-f shows the calculated field enhancement of core-shell structures and solid Au nanospheres as a function of the incident-field wavelength for incident-field intensities of 0.08, 0.3, and 8 TW/cm², respectively. For each corresponding incident-field intensity, Figure 4a-c compares a section of our simulated electric-field-

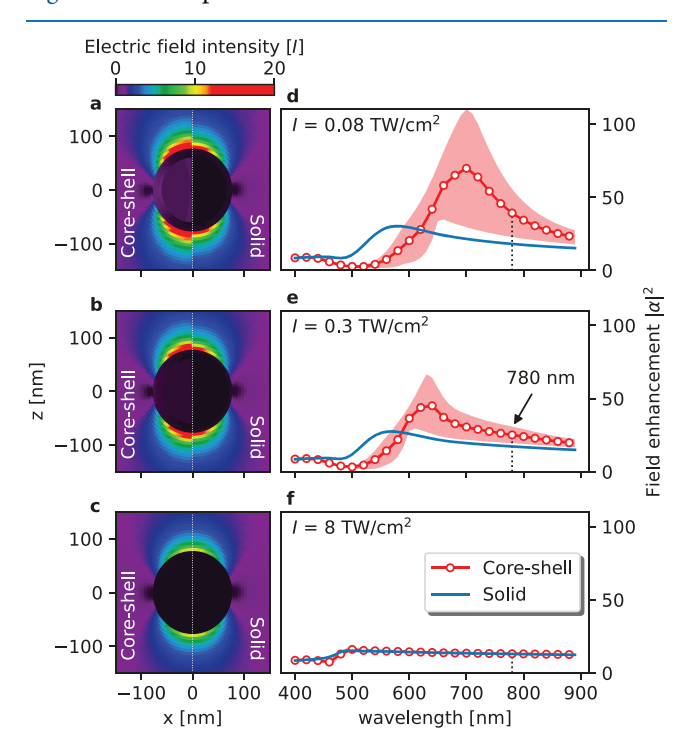


Figure 4. Controlling plasmonic properties of core—shell structures. (a–c) Simulated inhomogeneous electric-field intensity distribution for core—shell structures (left half) and solid Au nanospheres (right half), for the incident-field wavelength of 780 nm and intensities of (a) 0.08, (b) 0.3, and (c) 8 TW/cm². (d–f) Simulated field enhancement $|\alpha|^2$ as a function of incident wavelength, under the same respective incident-field intensities, for core—shell (red circled lines) and solid Au nanospheres (blue solid lines). The red shaded areas are the uncertainty range caused by the manufacturing dispersity of the inner and outer radii of the core—shell structures.

intensity distribution between the two types of nanoparticles for an incident field at 780 nm wavelength.

At 0.08 TW/cm², where the linear optical response dominates, a weak yet noticeable field penetrates the Au shell of the core–shell structure. The propagation of the external field across the ${\rm Au-SiO_2}$ interface yields the significantly more intense and red-shifted resonant spectra, as compared with solid Au nanoparticles. Such pronounced differences show that the plasmonic response of core–shell structures, including the absorption resonance and the nearfield magnitude, can be tuned by changing parameters in the production of the nanospheres (core diameter and shell thickness and composition).^{7–10}

As the incident-field intensity increases, due to the growing nonlinear response of the Au shell preventing penetration of the field, the resonance feature for the core-shell structures starts to blue-shift and decreases in magnitude, before gradually becoming indistinguishable from solid Au nanospheres across the spectra. We thus demonstrate that for coreshell nanoparticles, the tunable plasmonic response can be effectively switched "on" and "off" by simply controlling the external-field intensity. For intensities well below a threshold (\sim 2 TW/cm² in this work), the tunable plasmonic response of core-shell structures is switched "on", manifesting a large and red-shifted resonance. For intensities above the threshold, the response is effectively switched "off", and the core-shell structures appear to be indistinguishable from the solid Au nanospheres. According to eq 3, for a chosen material, such a threshold is determined primarily by the shell thickness, where a thinner shell requires a larger intensity threshold to ensure that the IR skin depth is smaller than the shell thickness. This shows that core-shell nanoparticles can be carefully synthesized to have a designated intensity threshold so that their plasmonic properties are controllable by manipulating the external-field intensity.

CONCLUSIONS

We have demonstrated the ability to control the plasmonic response of a layered nanostructure solely by varying the laser intensity. This was accomplished by measuring the photoelectron cutoff energies from single, isolated core-shell nanoparticles and using them as a sensitive probe of the plasmonic field. Experimental signatures of a non-constant, intensity-dependent near-field were verified by a modified Mie theory as the direct result of the nonlinear optical response of the outer gold shell. Further analysis revealed that the decreasing skin depth into the nanoparticle surface at laser intensities above $\sim 2 \text{ TW/cm}^2$ effectively shields the SiO₂ core, rendering the magnitude of its near-field identical to that of a solid Au nanosphere. These results suggest a new intensitydependent strong-field control of the plasmonic response in layered nanostructures. Although such responses in layered nanostructures are known to be tunable by their physical structure, we demonstrated that they can further be effectively switched "on" and "off" solely by controlling the external-field

This intensity-dependent optical control of the plasmonic response could hold the key to new lines of research and implementations based on layered nanostructures. For example, many applications require nanosystems such as core—shell structures to be tuned to precise resonant wavelengths. 9,10 Our work unlocks a new tuning mechanism where a core—shell (or layered) structure can be manipulated

to have adjustable resonance and optical properties, dependent merely on the applied laser intensity, without modifying its shape, size, or material. In other applications, such as photocatalysis and field-induced molecular reactions, core—shell structures could be versatile substitutes for the currently used solid nanoparticles. Not only can they be tailored to provide larger field enhancements and substantially reduce the laser intensity requirements but such large enhancements can also be automatically turned "off" by the nonlinear response to avoid overexposure at high intensities. This can have significant impacts in areas such as metamaterials, plasmonics, and opto-electronics.

ASSOCIATED CONTENT

Supporting Information

The Supporting Information is available free of charge at https://pubs.acs.org/doi/10.1021/acsphotonics.2c00663.

Details of the experimental setup, data analysis, and simulation methods (ZIP)

AUTHOR INFORMATION

Corresponding Authors

Jeffrey A. Powell — J. R. Macdonald Laboratory, Department of Physics, Kansas State University, Manhattan, Kansas 66506, United States; Department of Physics, University of Connecticut, Storrs, Connecticut 06269, United States; INRS, Énergie, Matériaux et Télécommunications, Varennes, Québec J3X 1P7, Canada; orcid.org/0000-0002-3340-0890; Email: jeffrey.powell@inrs.ca

Jianxiong Li − J. R. Macdonald Laboratory, Department of Physics, Kansas State University, Manhattan, Kansas 66506, United States; Louisiana State University, Baton Rouge, Louisiana 70803, United States; oorcid.org/0000-0002-5281-7114; Email: jasonli3@lsu.edu

Authors

Adam Summers – J. R. Macdonald Laboratory, Department of Physics, Kansas State University, Manhattan, Kansas 66506, United States; SLAC National Accelerator Laboratory, Menlo Park, California 94025, United States

Seyyed Javad Robatjazi – J. R. Macdonald Laboratory, Department of Physics, Kansas State University, Manhattan, Kansas 66506, United States

Michael Davino – Department of Physics, University of Connecticut, Storrs, Connecticut 06269, United States

Philipp Rupp – Physics Department, Ludwig-Maximilians-Universität Munich, D-85748 Garching, Germany

Erfan Saydanzad – J. R. Macdonald Laboratory, Department of Physics, Kansas State University, Manhattan, Kansas 66506, United States

Christopher M. Sorensen – Department of Physics, Kansas State University, Manhattan, Kansas 66506, United States

Daniel Rolles – J. R. Macdonald Laboratory, Department of Physics, Kansas State University, Manhattan, Kansas 66506, United States; orcid.org/0000-0002-3965-3477

Matthias F. Kling — Physics Department, Ludwig-Maximilians-Universität Munich, D-85748 Garching, Germany; Max Planck Institute of Quantum Optics, D-85748 Garching, Germany; SLAC National Accelerator Laboratory, Menlo Park, California 94025, United States; Department of Applied Physics, Stanford University, Stanford, California 94305, United States; oorcid.org/0000-0002-1710-0775

Carlos Trallero – J. R. Macdonald Laboratory, Department of Physics, Kansas State University, Manhattan, Kansas 66506, United States; Department of Physics, University of Connecticut, Storrs, Connecticut 06269, United States

Uwe Thumm – J. R. Macdonald Laboratory, Department of Physics, Kansas State University, Manhattan, Kansas 66506, United States

Artem Rudenko – J. R. Macdonald Laboratory, Department of Physics, Kansas State University, Manhattan, Kansas 66506, United States

Complete contact information is available at: https://pubs.acs.org/10.1021/acsphotonics.2c00663

Author Contributions

J.A.P. and J.L. contributed equally to this work. J.A.P., J.L., A.S., U.T., and A.R. conceptualized and conducted the study. J.A.P., A.S., S.J.R, M.D., and P.R. contributed to performing the experiment. J.A.P. and A.S. performed the data analysis. J.L. and U.T. developed the theoretical model, performed the simulations, and interpreted the results. J.A.P., J.L., A.S., E.S., C.M.S., D.R., M.F.K., C.T.H., U.T., and A.R. discussed the results. J.L., J.A.P., and A.S. wrote the initial manuscript, which was revised with input from all authors.

Funding

This work was supported by the Air Force Office of Scientific Research under award number FA9550-17-1-0369. J.L., E.S.. and U.T. acknowledge support by NSF grants PHY 1802085 and PHY 2110633. A.S. and D.R. were supported by the Chemical Sciences, Geosciences, and Biosciences Division, Office of Basic Energy Sciences, Office of Science, the U. S. Department of Energy under Award No. DEFG02-86ER13491, which also covered laser operational costs. M.F.K. acknowledges support by the German Research Foundation (DFG) via SPP1840 and project no. 470372174, and the Max Planck Society via the Max Planck Fellow program. M.F.K.'s work at SLAC was supported by the U.S. Department of Energy, Office of Science, Basic Energy Sciences, Scientific User Facilities Division, under Contract No. DE-AC02-76SF00515.

Note:

The authors declare no competing financial interest. The data that support the findings of this study are available from the corresponding authors upon reasonable request. Code Availability: The code used to reproduce the results from this paper is available at https://github.com/jasonleekungfu/KSU.004.NL under the MIT License.

REFERENCES

- (1) Stockman, M. I. Nanoplasmonics: The physics behind the applications. *Phys. Today* **2011**, *64*, 39–44.
- (2) Law, S.; Yu, L.; Rosenberg, A.; Wasserman, D. All-Semi-conductor Plasmonic Nanoantennas for Infrared Sensing. *Nano Lett.* **2013**, *13*, 4569–4574.
- (3) Krausz, F.; Stockman, M. I. Attosecond metrology: from electron capture to future signal processing. *Nat. Photonics* **2014**, *8*, 205–213.
- (4) Sheldon, M. T.; van de Groep, J.; Brown, A. M.; Polman, A.; Atwater, H. A. Plasmoelectric potentials in metal nanostructures. *Science* **2014**, *346*, 828–831.
- (5) Zhang, X.; Chen, Y. L.; Liu, R.-S.; Tsai, D. P. Plasmonic photocatalysis. *Rep. Prog. Phys.* **2013**, *76*, 046401.

- (6) Wu, T.; Liu, S.; Luo, Y.; Lu, W.; Wang, L.; Sun, X. Surface plasmon resonance-induced visible light photocatalytic reduction of graphene oxide: Using Ag nanoparticles as a plasmonic photocatalyst. *Nanoscale* **2011**, *3*, 2142–2144.
- (7) Li, J.; Saydanzad, E.; Thumm, U. Imaging Plasmonic Fields with Atomic Spatiotemporal Resolution. *Phys. Rev. Lett.* **2018**, *120*, 223903.
- (8) Hirsch, L. R.; Gobin, A. M.; Lowery, A. R.; Tam, F.; Drezek, R. A.; Halas, N. J.; West, J. L. Metal Nanoshells. *Ann. Biomed. Eng.* **2006**, 34, 15–22.
- (9) Rastinehad, A. R.; et al. Gold nanoshell-localized photothermal ablation of prostate tumors in a clinical pilot device study. *Proc. Natl. Acad. Sci. U.S.A.* **2019**, *116*, 18590–18596.
- (10) Chen, W.; et al. Targeting of Pancreatic Cancer with Magneto-Fluorescent Theranostic Gold Nanoshells. *Nanomedicine* **2014**, *9*, 1209–1222.
- (11) Li, J.Spatiotemporally Resolved Photoemission from Plasmonic Nanoparticle. Ph.D. Thesis, Kansas State University, 2020.
- (12) Thomas, S.; Krüger, M.; Förster, M.; Schenk, M.; Hommelhoff, P. Probing of Optical Near-Fields by Electron Rescattering on the 1 nm Scale. *Nano Lett.* **2013**, *13*, 4790–4794.
- (13) Rácz, P.; Pápa, Z.; Márton, I.; Budai, J.; Wróbel, P.; Stefaniuk, T.; Prietl, C.; Krenn, J. R.; Dombi, P. Measurement of Nanoplasmonic Field Enhancement with Ultrafast Photoemission. *Nano Lett.* **2017**, 17, 1181–1186.
- (14) Deeb, C.; Zhou, X.; Plain, J.; Wiederrecht, G. P.; Bachelot, R.; Russell, M.; Jain, P. K. Size Dependence of the Plasmonic Near-Field Measured via Single-Nanoparticle Photoimaging. *J. Phys. Chem. C* **2013**, *117*, 10669–10676.
- (15) Süßmann, F.; et al. Field propagation-induced directionality of carrier-envelope phase-controlled photoemission from nanospheres. *Nat. Commun.* **2015**, *6*, 7944.
- (16) Powell, J. A.; Summers, A. M.; Liu, Q.; Robatjazi, S. J.; Rupp, P.; Stierle, J.; Trallero-Herrero, C.; Kling, M. F.; Rudenko, A. Interplay of pulse duration, peak intensity, and particle size in laser-driven electron emission from silica nanospheres. *Opt. Express* **2019**, 27, 27124–27135.
- (17) Zherebtsov, S.; et al. Controlled near-field enhanced electron acceleration from dielectric nanospheres with intense few-cycle laser fields. *Nat. Phys.* **2011**, *7*, 656–662.
- (18) Rupp, P.; et al. Few-cycle laser driven reaction nanoscopy on aerosolized silica nanoparticles. *Nat. Commun.* **2019**, *10*, 4655.
- (19) Bormann, R.; Gulde, M.; Weismann, A.; Yalunin, S. V.; Ropers, C. Tip-Enhanced Strong-Field Photoemission. *Phys. Rev. Lett.* **2010**, *105*, 147601.
- (20) Krüger, M.; Schenk, M.; Hommelhoff, P. Attosecond control of electrons emitted from a nanoscale metal tip. *Nature* **2011**, 475, 78–81.
- (21) Herink, G.; Solli, D. R.; Gulde, M.; Ropers, C. Field-driven photoemission from nanostructures quenches the quiver motion. *Nature* **2012**, 483, 190–193.
- (22) Li, J.; Saydanzad, E.; Thumm, U. Attosecond time-resolved streaked photoelectron spectroscopy of transition-metal nanospheres. *Phys. Rev. A* **2017**, *95*, 043423.
- (23) Saydanzad, E.; Li, J.; Thumm, U. Strong-field ionization of plasmonic nanoparticles. *Phys. Rev. A* **2022**, *106*, 033103.
- (24) Xiao, Y.; Qian, H.; Liu, Z. Nonlinear Metasurface Based on Giant Optical Kerr Response of Gold Quantum Wells. *ACS Photonics* **2018**, *5*, 1654–1659.
- (25) Nookala, N.; Lee, J.; Tymchenko, M.; Sebastian Gomez-Diaz, J. S.; Demmerle, F.; Boehm, G.; Lai, K.; Shvets, G.; Amann, M.-C.; Alu, A.; Belkin, M. Ultrathin gradient nonlinear metasurface with a giant nonlinear response. *Optica* **2016**, *3*, 283–288.
- (26) Kauranen, M.; Zayats, A. V. Nonlinear plasmonics. *Nat. Photonics* **2012**, *6*, 737–748.
- (27) Kling, N. G.; Paul, D.; Gura, A.; Laurent, G.; De, S.; Li, H.; Wang, Z.; Ahn, B.; Kim, C. H.; Kim, T. K.; Litvinyuk, I. V.; Cocke, C. L.; Ben-Itzhak, I.; Kim, D.; Kling, M. F. Thick-lens velocity-map

- imaging spectrometer with high resolution for high-energy charged particles. *J. Instrum.* **2014**, *9*, P05005.
- (28) Summers, A. M.Strong-Field Interactions in Atoms and Nanosystems: Advances in Fundamental Science and Technological Capabilities of Ultrafast Sources. Ph.D. Thesis, Kansas State University, 2019.
- (29) Powell, J.Strong-Field Driven Dynamics of Metal and Dielectric Nanoparticles. Ph.D. Thesis, Kansas State University, 2017.
- (30) Mie, G. Beiträge zur Optik trüber Medien, speziell kolloidaler Metallösungen. *Ann. Phys.* **1908**, *330*, *377*–445.
- (31) Stratton, J.Electromagnetic Theory; Wiley, 2007; Vol. 33; pp 563-567.
- (32) Johnson, P. B.; Christy, R. W. Optical Constants of the Noble Metals. *Phys. Rev. B: Solid State* **1972**, *6*, 4370–4379.
- (33) Palik, E.Handbook of Optical Constants of Solids; Elsevier Science, 1985; p 275.
- (34) Aden, A. L.; Kerker, M. Scattering of Electromagnetic Waves from Two Concentric Spheres. J. Appl. Phys. 1951, 22, 1242–1246.
- (35) Ladutenko, K.; Pal, U.; Rivera, A.; Peña-Rodríguez, O. Mie calculation of electromagnetic near-field for a multilayered sphere. *Comput. Phys. Commun.* **2017**, *214*, 225–230.
- (36) Wang, Z.; Camacho Garibay, A.; Park, H.; Saalmann, U.; Agostini, P.; Rost, J. M.; DiMauro, L. F. Universal High-Energy Photoelectron Emission from Nanoclusters Beyond the Atomic Limit. *Phys. Rev. Lett.* **2020**, *124*, 173201.
- (37) Schötz, J.; Seiffert, L.; Maliakkal, A.; Blöchl, J.; Zimin, D.; Rosenberger, P.; Bergues, B.; Hommelhoff, P.; Krausz, F.; Fennel, T.; Kling, M. F.Onset of space-charge effects in strong-field photocurrents from nanometric needle tips, **2021**. arXiv:2106.00503.
- (38) Süßmann, F.; Kling, M. F. Attosecond nanoplasmonic streaking of localized fields near metal nanospheres. *Phys. Rev. B: Condens. Matter Mater. Phys.* **2011**, 84, 121406.
- (39) Li, J.; Saydanzad, E.; Thumm, U. Retrieving plasmonic near-field information: A quantum-mechanical model for streaking photoelectron spectroscopy of gold nanospheres. *Phys. Rev. A* **2016**, 94, 051401.
- (40) Boyd, R. W. Nonlinear Optics; Academic Press, 2008; p 210.
- (41) Boyd, R. W.; Shi, Z.; De Leon, I. D. The third-order nonlinear optical susceptibility of gold. *Opt. Commun.* **2014**, *326*, 74–79.
- (42) Qian, H.; Xiao, Y.; Liu, Z. Giant Kerr response of ultrathin gold films from quantum size effect. *Nat. Commun.* **2016**, *7*, 13153.
- (43) Hecht, E. Optics, 4th ed.; Addison-Wesley: Reading, MA, 2002; p 128.
- (44) Myroshnychenko, V.; Rodríguez-Fernández, J.; Pastoriza-Santos, I.; Funston, A. M.; Novo, C.; Mulvaney, P.; Liz-Marzán, L. M.; García de Abajo, F. J. Modelling the optical response of gold nanoparticles. *Chem. Soc. Rev.* **2008**, *37*, 1792–1805.
- (45) Yabana, K.; Sugiyama, T.; Shinohara, Y.; Otobe, T.; Bertsch, G. F. Time-dependent density functional theory for strong electromagnetic fields in crystalline solids. *Phys. Rev. B: Condens. Matter Mater. Phys.* **2012**, *85*, 045134.
- (46) Floss, I.; Lemell, C.; Wachter, G.; Smejkal, V.; Sato, S. A.; Tong, X.-M.; Yabana, K.; Burgdörfer, J. Ab initio multiscale simulation of high-order harmonic generation in solids. *Phys. Rev. A* **2018**, 97, 011401.
- (47) Rosenberger, P.; et al. Near-Field Induced Reaction Yields from Nanoparticle Clusters. ACS Photonics 2020, 7, 1885–1892.